POLITECNICO DI TORINO
Repository ISTITUZIONALE

Development and validation of the 4C thermal–hydraulic model of the ITER Central Solenoid modules

Original
Development and validation of the 4C thermal–hydraulic model of the ITER Central Solenoid modules / Zappatore, A.; Bonifetto, R.; Martovetsky, N.; Zanino, R.. - In: CRYOGENICS. - ISSN 0011-2275. - ELETTRONICO. - 127:(2022), p. 103552. [10.1016/j.cryogenics.2022.103552]

Availability:
This version is available at: 11583/2975550 since: 2023-02-21T16:42:22Z

Publisher:
ELSEVIER SCI LTD

Published
DOI:10.1016/j.cryogenics.2022.103552

Terms of use:

This article is made available under terms and conditions as specified in the corresponding bibliographic description in the repository

Publisher copyright
Elsevier postprint/Author's Accepted Manuscript

© 2022. This manuscript version is made available under the CC-BY-NC-ND 4.0 license
http://creativecommons.org/licenses/by-nc-nd/4.0/.The final authenticated version is available online at:
http://dx.doi.org/10.1016/j.cryogenics.2022.103552

(Article begins on next page)

23 April 2024

Development and validation of the 4C thermal-hydraulic model of the ITER Central Solenoid Modules

A. Zappatore,[a] R. Bonifetto,[a,*] N. Martovetsky[b] and R. Zanino[a]

[a]*NEMO group, Dipartimento Energia "Galileo Ferraris", Politecnico di Torino, Torino, Italy*

[b]*Lawrence Livermore National Laboratory, on assignment to Oak Ridge National Laboratory, USA*

*E-mail: roberto.bonifetto@polito.it

Abstract

The ITER Central Solenoid (CS) consists of a stack of six modules, each made of 40 pancakes wound with Nb3Sn Cable-In-Conduit Conductors (CICCs) cooled with supercritical helium (SHe). All six modules (plus one spare) are to be individually cold-tested at the General Atomics final test facility in San Diego (USA), in order to check their performance; the first CS Module (CSM1) was tested in early 2020.

A test campaign on a CSM Mock-up (CSM MU) wound with 16 dummy pancakes, i.e., with non-superconducting (copper) strands, was already carried out in San Diego at the end of 2017, for the commissioning of the test facility. The analysis of the CSM MU experimental data is presented here.

Each CSM is a full magnet with 554 turns; it did not have any thermal-hydraulic (TH) or electrical sensors inside the winding due to insulation reasons, so that, e.g., SHe pressure, temperature and mass flow rate, as well as the voltage, were only measured at the ends of selected pancakes.

Therefore, it was essential to employ a thermal-hydraulic (TH) model in order to obtain information on the quantities of interest inside the coil, e.g. which was the voltage across the coil at the moment when the current sharing temperature (T_{CS}) was reached for the first time somewhere in that double-pancake (DP) during a T_{CS} test.

The TH model of the CSM, developed and implemented in the validated 4C code, and eventually adopted for the test preparation and interpretation, includes some free parameters, i.e., the inter-pancake and inter-turn thermal coupling, whose uncertainty is mainly due to the complex, multi-layer structure of the turn and pancake insulation. The calibration of these parameters is required to correctly capture the TH behavior of the CSM. For this purpose, the results of the experimental campaign on the CSM MU have been used. The detailed topology of the CSM MU is described and implemented here in a dedicated 4C model. Both slow and fast transients are used for the calibration, e.g., quasi-steady state heating of the SHe, entering a single DP and heat slug tests, respectively. It is shown that the transverse heat transfer within the winding pack could be largely overestimated if the ideal heat conduction across a bulk insulation layer is considered. The calibrated model is then validated on the CSM1 test results.

Keywords: Fusion; ITER; Modeling; Superconducting magnets; Thermal-hydraulic.

Acknowledgement

The work was financially funded by UT-Battelle under contract #534/2016

List of acronyms

CICC	Cable-In-Conduit Conductor
CS	Central Solenoid
CSI	Central Solenoid Insert
CSM	Central Solenoid Module
CSM MU	Central Solenoid Module Mock-up
DP	Double Pancake
HP	Hexa Pancake
IP	Inter-Pancake
IT	Inter-Turn
M_{IP}	Multiplier for Inter-Pancake heat transfer
M_{IT}	Multiplier for Inter-Turn heat transfer
P	Pancake
QP	Quad Pancake
Re	Reynolds number
SHe	Supercritical Helium
T_{CS}	Current Sharing Temperature
TH	Thermal-Hydraulic

I. Introduction

The US ITER domestic agency is responsible for the procurement of the 6 (+1 spare) modules of the ITER Central Solenoid (CS) [1]. A dedicated facility for the assembly process of each module has been built at General Atomics, Poway (CA), USA [2]. Before shipping them to the ITER site, each CS module (CSM) is planned to be cold tested at 4.5 K. To qualify the entire facility and especially the test station, a CSM Mock-Up (CSM MU) was assembled and tested. The CSM MU is pancake wound and consists of 2 hexa-pancakes (HP) and 1 quad-pancake (QP), see Figure 1. Each HP and the QP are made by a single conductor. They are electrically connected in series through joints.

From the hydraulic point of view, each couple of pancakes, typically called double-pancake (DP), is equipped with a SHe inlet. Each pancake (or "P" for brevity) is cooled in parallel to the others and each turn is in counter-flow with respect to the adjacent ones. The CSM MU features all the characteristics of a CSM, except for the number of pancakes (16 in the MU, 40 in each CSM) and for the strand material, which is copper in the MU whereas it is Nb_3Sn and copper as in the CSM.

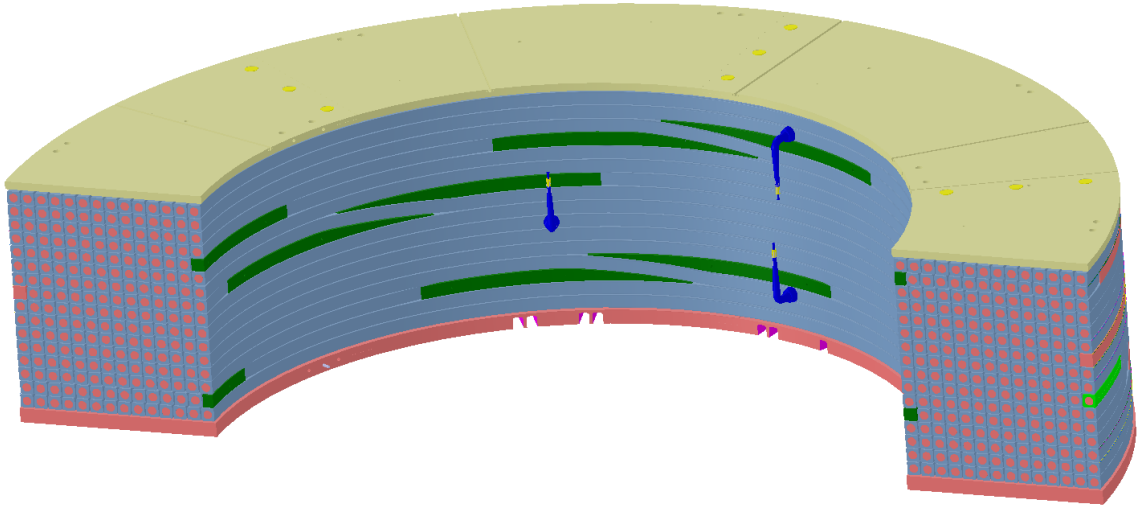

Figure 1 – CAD section of the CS module mockup, showing the 16 pancakes in gray, the He inlets in blue, the fillers at the pancake transitions in dark green, an inter-pancake electrical joint in light green on the right.

Since all modules will be instrumented only at their DPs inlets and outlets, to know what is going on inside the winding pack, the computational tools are needed.

The 4C code [3] is being employed for the thermal-hydraulic (TH) analysis of the tests performed on the modules. However, in order to be capable of capturing correctly the TH behavior of the CSMs, the 4C model needs the calibration of a few free parameters, such as those adopted in the inter-turn and inter-pancake thermal coupling model. For this purpose, the results of the experimental campaign on the CSM MU are used. The calibration of the model is carried out applying a down-sized version of the CSM model to the CSM MU, which was tested at the end of 2017.

In this paper, after a brief description of the experimental setup and results of the CSM MU tests relevant for the model calibration, the TH model of the CSM MU and the rigorous procedure for the calibration are presented. The model is then calibrated and then validated on another, independent set of CSM MU experimental tests, as well as against data collected during the first CSM (CSM1) campaign, at the beginning of 2020. Indeed, this is the first time the model of the thermal coupling among different conductors implemented in the 4C code is calibrated and validated in a controlled case on an ITER magnet.

II. Experimental setup and results

In this section, the experimental setup and the results relevant for the following analysis are

described.

II.A. Experimental setup

The CSM MU was cooled with SHe at ~ 5 bar and ~ 4.5 K with a mass flow rate of ~ 10 g/s/pancake.

The CSM MU was equipped with two so-called "T_{CS} loops", i.e. inlet pipes (each feeding a DP) with a resistive heater used to increase the He inlet temperature, a mass flow meter, a pressure and a temperature sensor. The first two are located upstream with respect to the heater, while the latter is located downstream. The upstream temperature is measured by a temperature sensor (TT157) located on the supply line. The inlets of P5-P6 and P9-P10 each featured a T_{CS} loop, see Figure 2. All the outlet pipes, collecting the SHe coming from a DP, are equipped with a temperature sensor, except for P1 and P16. The SHe is fed to each DP, by a single inlet and it is recollected by two different outlet pipes, e.g. the He flowing in P8 is fed by an inlet which is common to P7 and P8, while it is recollected by a pipe that is common to P8 and P9, see Figure 2. This will be an important feature in the discussion of the results.

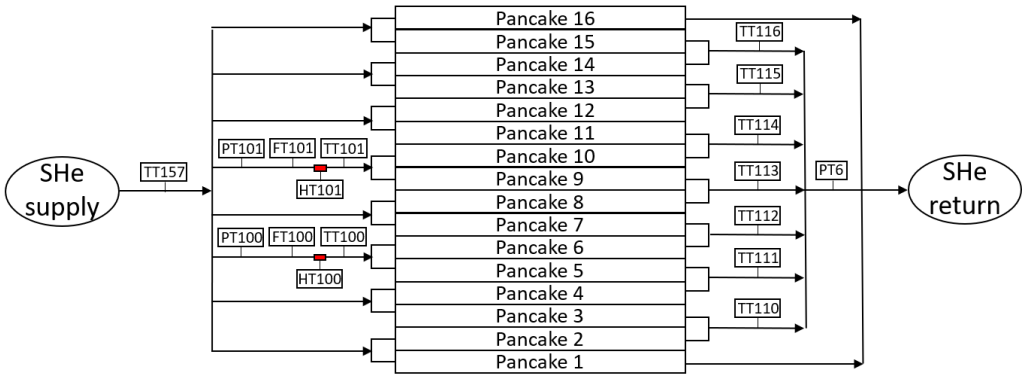

Figure 2 – Detail of the mock-up P&ID. The location of pressure (PT), mass flow rate (FT) and temperature (TT) sensors, as well as that of the resistive heaters (HT), is shown.

II.B. Experimental results

Among the different objectives of the CSM MU test campaign there was also the collection of data useful for the calibration of the thermal-hydraulic models planned to be adopted for the analysis of the subsequent test campaign on the CSMs. A summary of the tests relevant for the calibration of thermal-hydraulic codes is reported in Table 1. The shots identified with HT0_## and with HT1_## were performed firing heaters HT100 and HT101, respectively.

Table 1 - Overview of the thermal-hydraulic tests for code calibration.

Shot	Maximum heater power (W)	Mass flow rate (g/s)	Description of the shot
HT0_01	300	5.0	Steady state up to 300 W
HT1_01	100	4.0	Steady state at 100 W
HT0_02	280	5.0	T_{CS}-like scenario
HT1_02	300	4.0	Steady state up to 300 W
HT1_03	200	4.0	T_{CS}-like scenario
HT0_03	100	5.0	Steady state at 50 W and 100 W
HT0_15	180	5.5	Steady state up to 180 W
HT0_16	350	4.0	T_{CS}-like scenario

HT0_17	300	7.5	T_{CS}-like scenario
HT0_04	75	5.5	Heat slug (pulse duration: 93 s)
HT0_05	100	5.5	Heat slug (pulse duration: 75 s)
HT0_06	200	5.5	Heat slug (pulse duration: 98 s)
HT0_07	100	5.5	Heat slug (pulse duration: 150 s)
HT0_08	200	5.5	Heat slug (pulse duration: 150 s)
HT0_09	200	8.0	Heat slug (pulse duration: 153 s)
HT0_10	200	8.2	Heat slug (pulse duration: 190 s)
HT0_11	200	8.3	Heat slug (pulse duration: 360 s)
HT0_12	300	8.1	Heat slug (pulse duration: 140 s)
HT0_13	300	8.1	Heat slug (pulse duration: 182 s)
HT0_14	300	8.2	Heat slug (pulse duration: 241 s)
HT1_04	100	4.4	Heat slug (pulse duration: 150 s)
HT1_05	200	4.4	Heat slug (pulse duration: 150 s)
HT1_06	300	7.6	Heat slug (pulse duration: 245 s)
HT1_07	200	7.5	Heat slug (pulse duration: 365 s)

The free parameters which need calibration are embedded in the inter-turn (IT) and inter-pancake (IP) thermal coupling model. The latter involves the heat transfer along the entire pancake length; therefore, for its calibration it is useful to have long plateaus, i.e., longer than a pancake transit time (~1000 s in the nominal operating conditions). This was achieved holding the heater power constant for ~ 2000 s, see Figure 3(a-b). The heater power was then increased to another power level and held for the same time interval, leading to a staircase-like heating scenario. The evolution of the mass flow rate in the directly heated inlet pipe shows that the larger the heater power the lower the mass flow rate. On the other hand, the effect on the mass flow rate on a non-heated inlet pipe is negligible, because the decrease in the mass flow rate of the directly heated pipe is redistributed among all the other inlet pipes. The temperature level measured at the outlet, see Figure 3(b), depends on how strong or weak is the thermal coupling between adjacent pancakes, and it is therefore useful for the calibration of the IP thermal coupling. The evolution of the outlet temperatures of pancakes that are symmetric with respect to the heated DP is basically the same, e.g., TT111 and TT112, TT110 and TT113 and so on. This behavior means that the IP thermal coupling is uniform throughout the coil. The shot discussed so far will be identified in the following as HT0_01.

An independent shot is then used as a cross-check of the calibrated value obtained on the shot described above. To this purpose, another "long" shot was selected (HT0_02). It was a T_{CS}-like heating scenario, whose aim was mainly to qualify the test facility for T_{CS} tests on the CSM. The increase of the power and, therefore, of the inlet temperature was faster than in HT0_01, see Figure 3(c-d). Other "long" tests were performed, see *Table 1*, however they were less optimal for the purpose of the calibration and/or cross-check: HT1_02 had too fast plateau, i.e., not long enough to reach steady state outlet temperature; HT1_03 reached only 200 W, thus a lower temperature at the outlet was reached; in shot HT0_03 the heater was operated only at two values, thus reaching only two different outlet temperatures; HT0_15 has a feature similar to HT1_03 as it reached only 180 W; HT0_16 and HT0_17 had large heater oscillations, as they were intended more to optimize the strategy for the T_{CS} tests in the real module.

The IT thermal coupling is calibrated through faster heat slug tests, as it involves thermal coupling between single turns (much shorter than a pancake) and their two neighbors. In particular, the slug considered here was selected among those with:

- nominal mass flow rate, i.e. ~8 g/s/pancake, in order to be as close as possible to the real operating conditions;
- temperature increase at the outlet of the directly heated pancakes ≥ 1 K, i.e. heater flat top ~ 200 W, in order to have a reliable reading of the temperature sensors.

Therefore, the heat slug test chosen for the calibration is HT0_10, see Figure 3(e-f). The amplitude of the heat pulse leads to a stronger reduction of the mass flow rate in the directly heated pipe than in the HT0_01 shot and the effect (increase) on the mass flow rate of "101" inlet pipe is visible. The outlet temperature signals allow also to observe the transit time in each DP and a small difference is present between adjacent DPs. Furthermore, the directly heated pancakes, in turn, transfer heat to those adjacent to

them and this is visible in the outlet temperature signals TT110 and TT113.

The cross-check of the calibrated value is then performed on a similar heat slug, i.e., 200 W, but using the other T_{CS} loop (shot HT1_07).

Other heat slug tests were performed, see *Table 1*, but we excluded for our purposes those with too low heater power, i.e., smaller than 200 W, which led to a small outlet temperature increase. On the other hand, those carried out at 300 W reached almost choked flow condition at the inlet, thus we selected those at 200 W with a mass flow rate close to 8 g/s/pancake.

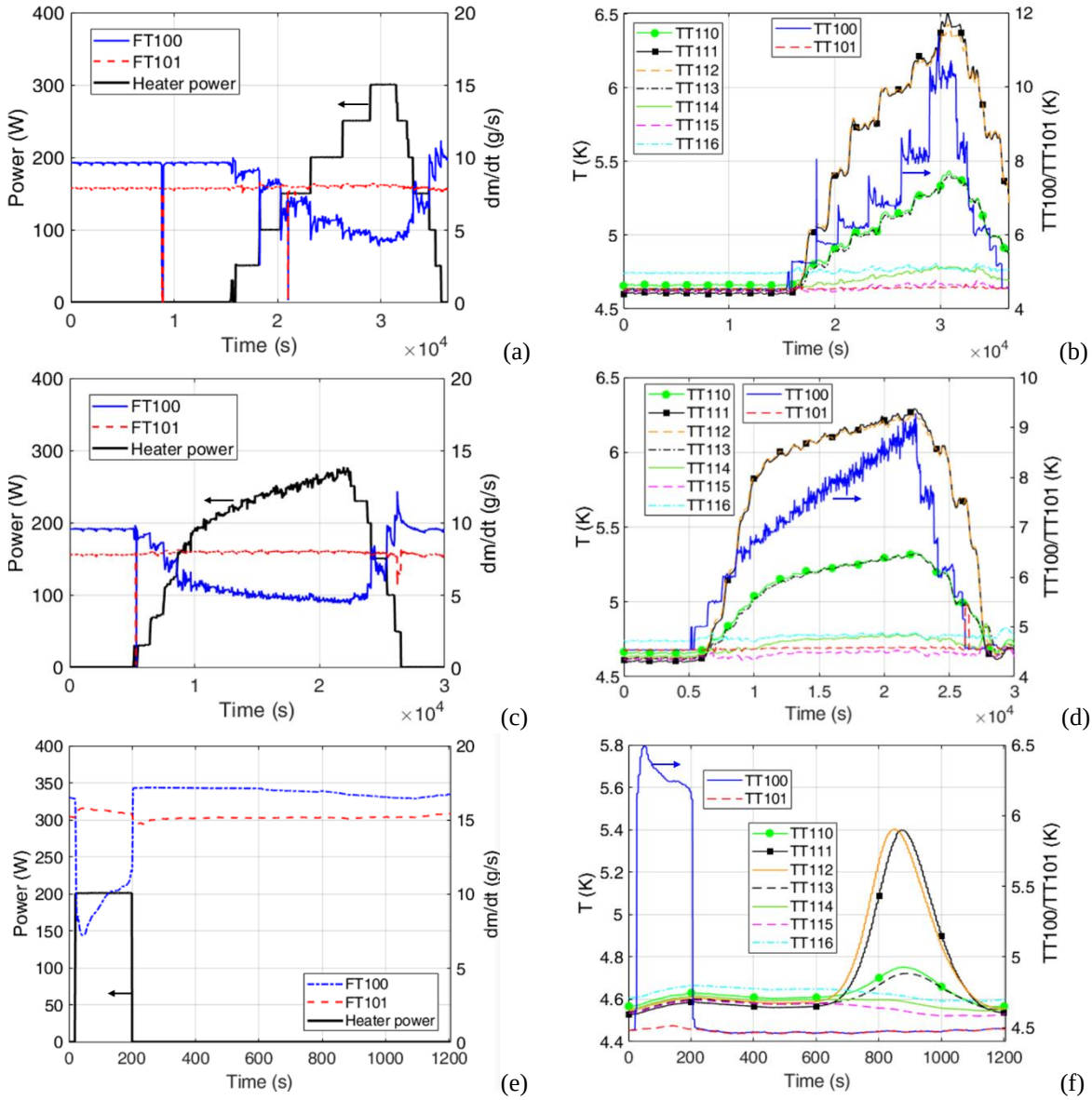

Figure 3 – TH tests performed on the CSM MU. Evolution of heater power and measured inlet mass flow rates for the staircase (shot HT0_01) (a) and T_{CS}-like (shot HT0_02) (c) heating scenarios and for a heat slug (shot HT0_10) (e). The corresponding measured inlet and outlet temperatures are reported in (b) for shot HT0_01, (d) for shot HT0_02 and (f) for shot HT0_10, respectively.

III. 4C model of the CSM MU

The analysis includes all 16 conductors, thermally coupled within the winding pack, and the cooling circuit. Therefore, two modules of the 4C code are exploited in this analysis: the winding pack module, based on the M&M code [4] and the cryogenic circuit module [5], based on the Modelica programming language [6]. The former solves the 1D compressible Euler-like set of equations for the He

flow in each hydraulic channel (two – the cable bundle region and the central channel – for each pancake) and the 1D heat conduction equations for the solids, i.e. the strands and the jacket. The latter includes 1D and 0D components (pipes, valves, manifolds, etc), where the mass, momentum and energy conservation equations are solved. The two modules are then suitably coupled and synchronized by means of the TISC® platform [7].

III.A. Winding model

The main characteristics of the CSM MU conductor implemented in the 4C code are those of the ITER CS Insert coil, see [8], and are reported in *Table 2*.

Table 2 – Main parameters of the CSM MU (representative of the CS coil modules)

Parameter	**Value**
Number of turns (-)	14
Cable diameter (mm)	33.0
Jacket external side (mm)	49
He cross section in the annulus (mm^2)	247.96
Void fraction in the annulus, φ (%)	33.6
Wetted perimeter of the annulus (twisted strands) (m)	1.9226
Central channel ID/OD (mm)	7 / 9
Friction factor correlation* (bundle) (-)	$(0.051+24.7/Re_b^{0.847})/(\varphi^{0.72})$ where Re_b is the Reynolds number[%]
Friction factor correlation* (central channel) (-)	$0.0958\times Re_h^{-0.181}$, where Re_h is the Reynolds number[&]

* Developed before Central Solenoid Insert (CSI) test campaign [8], based on short samples of CS conductor.

[%] $Re_b = \rho_b \cdot v_b \cdot D_b/\mu_b$, where ρ_b and μ_b are the density and dynamic viscosity, respectively, computed at the pressure and temperature of the He in the bundle, v_b is the He velocity in the bundle, D_b is the hydraulic diameter of the bundle.

[&] $Re_h = \rho_h \cdot v_h \cdot D_h/\mu_h$, where ρ_h and μ_h are the density and dynamic viscosity, respectively, computed at the pressure and temperature of the He in the central channel, v_h is the He velocity in the central channel, D_h is the inner diameter of the spiral.

III.A.1. Inter-turn and inter-pancake thermal coupling

III.A.1.a. Topology

The 4C code accounts for thermal coupling between adjacent turns and pancakes through the IT and IP insulation, respectively.

The (ground) insulation and support structures outside of the CSM MU winding are not included in the model.

It is useful here to make a distinction between the "pancake" and the "hydraulic channel" ("chan" for brevity). A "pancake" is typically identified as the portion of conductor whose axis lies on a given horizontal plane (same z-coordinate), see P14 to P16 in Figure 4. A "hydraulic channel" is the region of the conductor included between an inlet and an outlet and in which the SHe has always the same direction (clockwise or counter clockwise, if seen from the top). Typically, in thermal-hydraulic modelling of coils, pancakes and hydraulic channels are assumed to be the same. However, the distinction is relevant here because each DP has a single inlet in correspondence of the z-coordinate of one of the two pancakes,

therefore two adjacent hydraulic channels have different lengths with respect to the lengths of the two pancakes, e.g., the hydraulic length at the innermost *radial* coordinate of chan15 is much smaller that of chan16, see the regions highlighted in yellow and red in Figure 4: chan15 runs at the innermost radial coordinate only for ~ 1/4 of one turn, while chan16 covers the remaining 3/4 at the P15 z-coordinate and, after the transition, it runs for an entire turn length at the innermost radial coordinate at the P16 z-coordinate. This is important, for example, in case of the simulation of T_{CS} tests, because of the different hydraulic channel length at the peak magnetic field (uniform at the innermost turn).

The topology of the coil has been implemented with a great amount of details in the model. A much simpler approach could have been possible only if an "ideal" topology was present, e.g., if all the hydraulic channels had the same length and if they were thermally coupled with the same (neighbouring) pancakes along the entire length of the channel considered. Since in the real case under analysis each hydraulic channel is different with respect to the others, a different, more detailed approach has been preferred.

To illustrate the details of the topology implemented in the model, let us focus on the CSM MU P16 and P15, see Figure 4. The inlet of chan16 is located at the z-coordinate of P15. Once the SHe enters chan16 from the common P15-P16 inlet, it travels counter clockwise for ~3/4 of a complete turn at the P15 level. In this first portion, the SHe in chan16 is exchanging heat with the SHe of the second turn of chan15 in counterflow and with that flowing in parallel flow in the second turn of chan16 (one pancake up) and with that in chan14 (one pancake down).

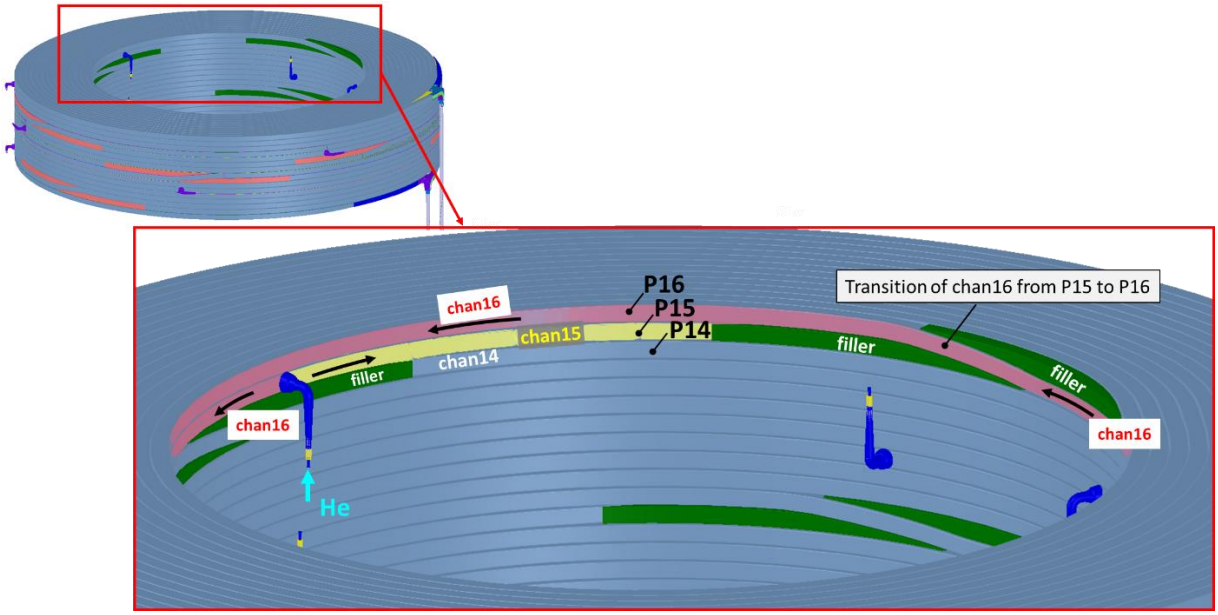

Figure 4 – In the top, CAD view of the CSM MU showing the 16 pancakes in gray, the fillers to assist the pancake transitions in dark green (inboard) and dark pink (outboard), He inlets and outlet in blue and purple, respectively. In the bottom, zoom of the top inboard region, showing the He flow direction in the He inlet, and highlighting the He flow direction in chan15 and chan16. The region where the transition of chan16 from P15 to P16 occurs is highlighted.

Continuing in the direction of SHe flow in chan16, it goes up at the P16 level, see the transition highlighted in Figure 4: the space left free by the conductor in the pancake-change region is occupied by a non-metallic filler, see the dark green regions in Figure 4. In this region, the thermal coupling with the portion of conductor below chan16 is neglected in the model for the entire filler length, in view of its insulation properties and of its thickness (equal to that of an entire CICC). Only after the pancake change from the P15 level to the P16 one, the SHe in chan16 has reached its "nominal" z-coordinate. From here on, the heat transfer is modelled as IT (parallel flow) thermal coupling within the same hydraulic channel and IP (counter flow) thermal coupling with chan15.

Note that:

- The different thickness of the IT (4 mm) and IP (3.5 mm) insulation is taken into account.

- The different turn length is considered: knowing the radial coordinate of the conductor centreline for each turn, the real turn length is considered.
- At the outermost turn, close to the SHe outlets, the real topology shows features similar to that at the innermost turn, with the same hydraulic channel possibly changing pancake level: the same level of detail explained above for the inlet region is modelled also there to properly account for the thermal coupling, even though here it is not relevant for the T_{CS} tests.
- The length needed to pass from one turn to the other is assumed to be zero, for the sake of simplicity. This assumption is justified by the fact that the "turn change" lasts only few tens of cm, therefore the error in the computation of the heat transfer in that region is expected to be very small.

This systematic approach allows having not only a very accurate map of the coil, i.e. an accurate description of the IT and IP thermal coupling, but also to take into account the real length of each hydraulic channel, which is (up to almost 10%) different for each pancake, see Table 3.

Table 3 – Hydraulic lengths of the CSM MU hydraulic channels.

Chan#	Hydraulic length (m)
1	147.25
2	143.72
3	148.61
4	143.96
5	146.94
6	145.83
7	148.37
8	145.64

Chan#	Hydraulic length (m)
9	147.41
10	139.79
11	144.47
12	143.23
13	150.82
14	143.42
15	150.97
16	153.57

III.A.1.b. Thermal coupling model

The thermal coupling between adjacent turns or pancakes is modelled through the thermal resistance given by the conduction through the turn or pancake insulation, and it is computed according to Eq. (1)

$$q'_{ideal} = HTC \cdot P_w \cdot (T_{jkt,A} - T_{jkt,B}) \quad (1)$$

where q'_{ideal} is the ideal (see below) power per unit length transferred between two adjacent hydraulic channels, say A and B, HTC is the heat transfer coefficient between A and B, P_w is the wetted perimeter, i.e., the jacket side, $T_{jkt,A}$ and $T_{jkt,B}$ are the jacket temperatures of the two channels. Note that, to compute q'_{ideal}, the *local* jacket temperatures should be employed. However, from the 1D model adopted in the simulations, only an average jacket temperature (for the jacket of each hydraulic channel) is computed. This assumption will lead to the computation of a q'_{ideal} that is larger than that computed with the local value of the temperature.

The heat transfer coefficient is computed as the inverse of the thermal resistance across the insulation thickness δ. *HTC* is computed according to Eq. (2)

$$HTC = \frac{k(T_{ins})}{\delta} \quad (2)$$

where k is the thermal conductivity of the insulation, evaluated at the (local) average temperature $T_{ins} = \frac{T_{jkt,A}+T_{jkt,B}}{2}$ of the jacket of the two adjacent portions of conductors.

The pure conduction approximation adopted in the thermal coupling model is known to overestimate the coupling, i.e., the effective thermal resistance is typically bigger than the bare conduction across the bulk insulating material [9]. This is known *a posteriori*, based on previous modelling experience, e.g. on the KSTAR PF coils [10], the EAST CS [9] and the JT-60SA CS [11], but also *a priori*, knowing

that the insulation is manufactured with a multi-layered structure (as discussed more in detail in Section IV.B.2), rather than a bulk material, whose thermal conductivity, k(T_{ins}), is known Therefore, the IT and IP thermal coupling need a dedicated calibration.

The actual (best fitting) heat flux will be given by

$$q'_{real} = M \cdot q'_{ideal} \tag{3}$$

where M is the calibration parameter, i.e. the multiplier of the ideal heat flux exchanged between turns (M = M_{IT}) or pancakes (M = M_{IP}). Based on the considerations above, together with the employment of the average jacket temperature rather than the local ones, *M* is expected to be within the interval (0,1).

III.B. Cooling Circuit Model

The model of the cooling circuit supplying SHe to the CSM (and CSM MU) has been built according to data available from the cryogenic circuit PID.

The supply and return pipes have been modelled lumping them in two equivalent lines (supply and return line in Figure 5), with an internal diameter of 46.3 mm and length equal to 28 m and 24 m, respectively, neglecting the elbows present in the pipelines. Both manifolds V1 and V2 have 0.1 m^3 volume.

The thickness of the cryoline pipes is assumed to be 1 mm, and the pipe wall material is stainless steel. The two heaters are modelled as 1 m long heated pipes where the power is deposited uniformly.

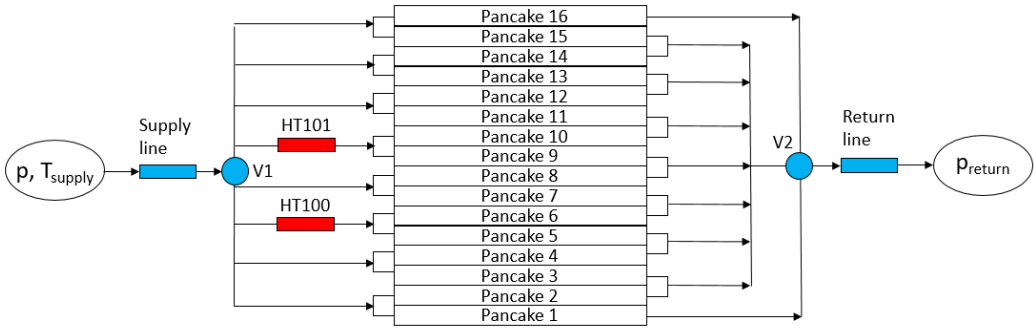

Figure 5 – 4C model of the CSM MU and its cooling circuit.

The circuit model is not closed (the cold circulator is not modelled) because during some tests the He was vented through a valve and the vented mass was not monitored. Therefore, we adopted a model in which we impose the pressure levels at the supply and return of the coil, from which (by means of the friction factor correlations in *Table 2*) the total mass flow rate circulating in the circuit is then computed.

IV. Calibration of the model free parameters

First, the IP thermal coupling is calibrated, using quasi-steady state runs. For this purpose, the best candidate is the HT0_01 shot, as discussed in Section II.B. Then, the calibrated value is frozen and the quality of the calibration is checked against another different shot. Note that in these long, quasi-steady runs the importance of the IT heat transfer is almost negligible, as the temperature difference between successive turns is relatively small (if compared to the temperature difference among neighbouring pancakes) and mainly driven by the SHe advection and IP heat transfer.

Then, the IT thermal coupling is calibrated on heat slugs following the same strategy and keeping the IP multiplier frozen, as it is not expected to be influenced by the transient timescale.

IV.A. Calibration of M_{IP}

In this section, the simulation setup for the calibration of the IP multiplier is presented. The rigorous calibration procedure, including a suitable quantitative definition of the error for the best-fitting procedure, is reported and the results are discussed.

IV.A.1. Simulation setup

Since the shot considered for the M_{IP} calibration is a series of long time intervals during which the inlet temperature of selected DPs is kept constant, the circuit is operated in steady state and its dynamics is not relevant; therefore, the model of the circuit around the coil is not considered for simplicity. The value of M_{IT} used in these simulations is 0, although, as discussed in the beginning of this section, its impact in quasi-steady state runs is negligible.

The boundary conditions considered for the M_{IP} calibration are the following:

- Experimental inlet mass flow rate (measured by FT100, see Figure 2, assumed equal also for the other DPs except for DP9-10, for which the measured FT101 was used)
- Experimental outlet pressure (PT6, see Figure 2)
- Inlet temperature to each pancake (TT157, see Figure 2)

Note that the measurement of the inlet temperature downstream the heater was not reliable, as confirmed by calorimetry and further dedicated tests after those performed on the CSM MU. This was due to the location of the temperature sensors, which was too close to the heater. This issue was then solved increasing the distance between end of the resistive heater and downstream temperature sensor before the tests of the actual modules.

A more reliable inlet temperature, adopted in the simulations, was deduced from the calorimetry itself: knowing the heater power, its inlet temperature and mass flow rate, it was possible to reconstruct the correct temperature downstream the heater, i.e., at the inlet of the heated DP. For this estimation, the mass flow rate measured by FT100 or FT101, depending on what heater was operated, was used; the inlet (cold) temperature was that of the common inlet (TT157), the pressure to compute the He enthalpy was taken from the sensor close to the heater, i.e., PT100 or PT101 and the heater power was taken from the electric signal. Knowing these quantities, the temperature downstream the heater was computed.

IV.A.2. Results

The calibration is based on the best-fitting of the coil outlet temperatures. Since each hydraulic channel is simulated, the outlet temperature of each pancake is computed. However, the sensors are located at the outlet of each *double*-pancake. Therefore, during the post-processing of the computed results, the resulting double-pancake outlet temperature is reconstructed, assuming adiabatic mixing between the outgoing SHe flow of two adjacent pancakes.

The evolution of the experimental outlet temperature increase is shown in Figure 6, and compared with that computed for selected M_{IP} values. Note that $\Delta T = TT11\#(t) - TT11\#(t=0)$ is shown, where $t = 0$ is the time right before the heater at the inlet is switched on. The use of the ΔT allows to cancel out the

presence of the static heat loads, coming from the supporting structure or from the cryostat, as well as any systematic offset of the temperature sensors.

From Figure 6, it is clear the strong effect of M_{IP} in the computed outlet temperatures: $M_{IP} = 0$ prevents the thermal coupling between directly heated pancakes P5-P6 (sensor TT112 - Figure 6a) and the unheated ones, e.g., P8-P9 (sensor TT113 - Figure 6b), which is clearly present in the experiment. As a result, $M_{IP} = 0$ leads to an overestimation of the outlet temperature of the directly heated pancakes.

Values of $M_{IP} > 0$ give more physical results, as the heat entering the directly heated pancakes is transferred to the adjacent "cold" ones: a temperature increase also at the outlet of indirectly heated pancakes is observed. Increasing the value of M_{IP}, e.g., $M_{IP} = 0.4$, the thermal coupling between adjacent pancakes starts to be overestimated: the outlet temperature of the directly heated pancakes is underestimated, while an overestimation of the outlet temperature of the indirectly heated ones is observed.

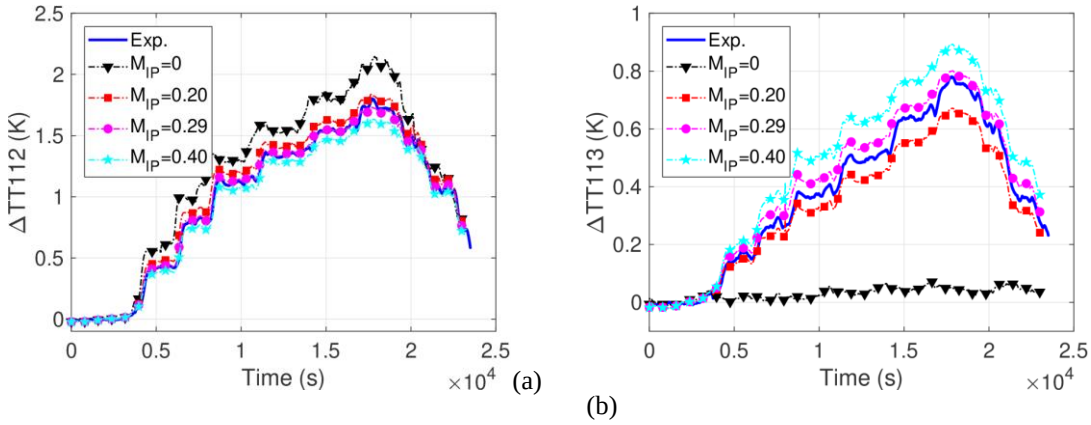

Figure 6 – Calibration of the IP thermal coupling multiplier M_{IP} on the shot HT0_01. Comparison of the experimental trace (solid line) with the computed results (dash-dotted lines) for different values of M_{IP} (symbols) for the sensors (a) TT112 (including a directly heated pancake) and (b) TT113 (including only indirectly heated pancakes), respectively, after the removal of the initial offset.

It is useful to focus on the steady state values of the outlet temperatures, i.e. the average values reached at the end of each power plateau.

The definition of the error adopted below is

$$Average\ error\ on\ \Delta T = 100 * \frac{\left|(T_{exp} - T_{exp,0}) - (T_{comp} - T_{comp,0})\right|}{\left|T_{exp} - T_{exp,0}\right|} \qquad (4)$$

where each T_{exp} and T_{comp} are evaluated as average during the final 500 s of each plateau and $T_{exp,0}$ and $T_{comp,0}$ are evaluated before turning on the heater. This definition is applied at each sensor for each plateau. Then, we take the average of the errors for all the plateaux, obtaining a single error value for each sensor. Finally, see below, a single (weighted) average value is obtained for all the sensors considered.

Figure 7(a) provides a summary of the comparison (in terms of average error) between experimental and computed plateau values of each outlet temperature sensor (without the initial offset) for the different values of M_{IP} tested parametrically in the model. It shows that different M_{IP} values lead to the smallest error on different sensors. However, an optimum value must be found: the optimum value is the one that globally minimizes the error on all the relevant sensors.

It is important to stress that to evaluate the global error, the contribution from each sensor has been weighted. The rationale is that the sensors TT111 and TT112 measure a higher (and clearer) signal than TT110 and TT113 and even more than TT114, which measures a much smaller temperature increase. The extreme case is, indeed, TT114, which gives a temperature increase so small that a very large average error would result with respect to the computed one, but only because the denominator in Eq. (4) is small. Therefore, the error on each sensor has been weighted with the ratio between the temperature increase of the sensor and the maximum temperature increase of all the sensors. This means that the TT111 and TT112 sensors will have weight = 1, while TT110 and TT113 will weigh 0.44 and TT114 will weigh only 0.08 on the global average error.

Figure 7(b) summarizes the comparison between the M_{IP} values analysed here, based on the global weighted error described above.

The value of M_{IP} = 0.29 minimizes the error with respect to the experimental values. This value is used below to cross-check on another (independent) shot the quality of the IP calibration performed here.

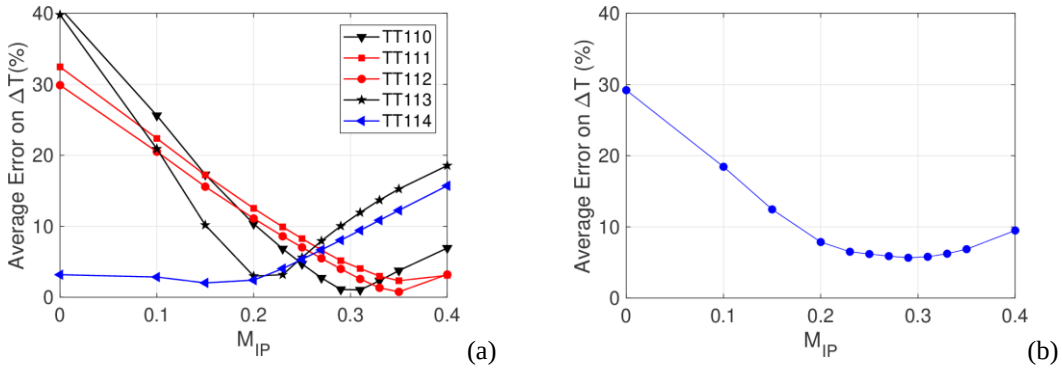

Figure 7 – Calibration of the IP thermal coupling multiplier M_{IP} on the shot HT0_01. (a) Average error for each sensor and (b) weighted error for all sensors as a function of M_{IP}.

IV.A.3. Validation

Since no other shots with long plateaus are available, except HT0_01, we chose for the cross-check of the M_{IP} value found above one of the slow T_{CS}-like transients, i.e. the HT0_02 shot.

Figure 8 shows the comparison of the measured and computed outlet temperature increase at selected sensors. The agreement of the measured and computed results is very good, i.e., within 0.05 K (4% error), therefore the recipe for the IP coupling can be considered to be fully validated for the CSM MU.

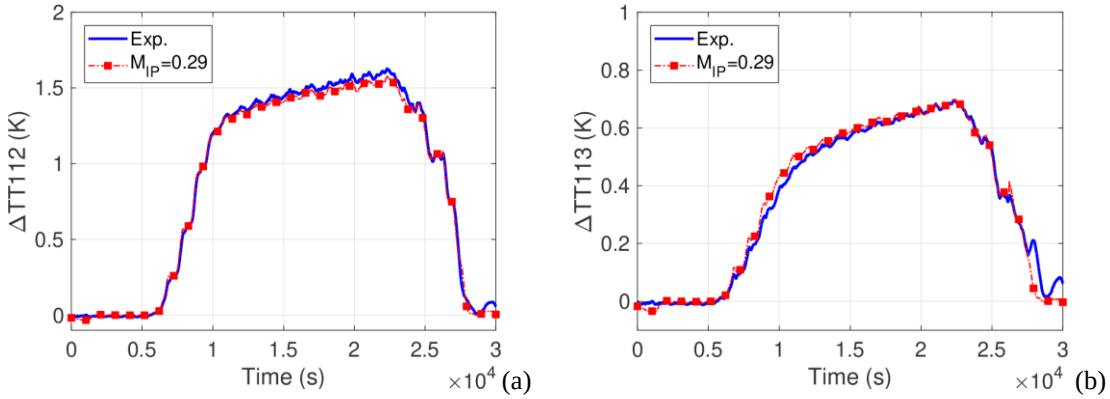

Figure 8 – Validation of the IP thermal coupling multiplier M_{IP} on the shot HT0_02. Comparison of the experimental evolution (solid line) with the computed results (dash-dotted line + squares) for the sensors (a) TT112 (including a directly heated pancake) and (b) TT113 (including only indirectly heated pancakes), respectively, without the initial offset.

IV.B. Calibration of M_{IT}

The calibration of the M_{IT} free parameter is performed on shot HT0_10. The M_{IP} parameter previously determined is frozen, therefore it is meaningful to calibrate a single free parameter on a different type of run.

The simulation setup and the results for the IT thermal coupling calibration are now discussed.

IV.B.1. Simulation setup

As already mentioned, the inlet temperature sensors give an unreliable measurement of the real SHe inlet temperature when the heater is operated. In the heat slug tests, which are faster transients than the staircase-like heating scenario, it is less reliable to employ a (steady-state) calorimetry to deduce the correct inlet He temperature. Therefore, it is necessary to include the heater in the model, assuming that the power measurement, i.e. the heater voltage and the current, is correct (as it is proven to be the case in long, staircase-like heating scenarios). This means that the model of (at least) a portion of the cooling circuit is needed.

In addition, during the heater operation (also during the long staircase and T_{CS}-like shots) the circuit is operated in nearly isobaric mode, i.e. SHe is loaded or unloaded depending on the pressure in certain positions of the circuit in order to keep it ~constant. However, the entering/exiting mass flow rate in/from the loop through the load/unload valve was not measured.

As a consequence, since we do not know the evolution of the total mass flow rate entering the CSM MU (the global mass flow rate is measured in the cryogenic facility only close to the cold circulator and does not account for the SHe load/unload flow), it is not possible to model the entire cooling loop, i.e., including the heat exchangers and the cold circulator: therefore, we cut the computational domain in correspondence to the inlet and outlet pressure sensors.

The boundary conditions of the model are, then, in this case, the inlet and outlet pressure and the inlet temperature. In particular:

- the inlet temperature (TT157, see Figure 2) is the measured one at the MU common inlet;
- the outlet pressure (PT6, see Figure 2) is the measured one from the MU common outlet;
- the inlet pressure is tuned, in order to compute the measured inlet mass flow rate. This was necessary because the available friction factor correlations were not able to predict the measured CSM1 hydraulic characteristic [12].

Concerning the inlet mass flow rate, right after the end of the heater operation an overshoot is expected, due to the incoming cold SHe at high pressure. This feature is present in all the heat slug tests at low mass flow rate (e.g. shot HT0_07) and correctly caught by the computational model, see Figure 9(a). However, in the heat slug tests with higher (nominal) mass flow rate, the overshoot is not present in the experiments, but still reproduced by the simulations, see Figure 9(b). This leads to the conclusion that the mass flow meter reaches its full scale value at 17.2 g/s, as it can be seen by the (non-physical) plateau from 200 s to 600 s, i.e. right after the end of the heater operation, in the HT0_10 shot, see again Figure 9(b).

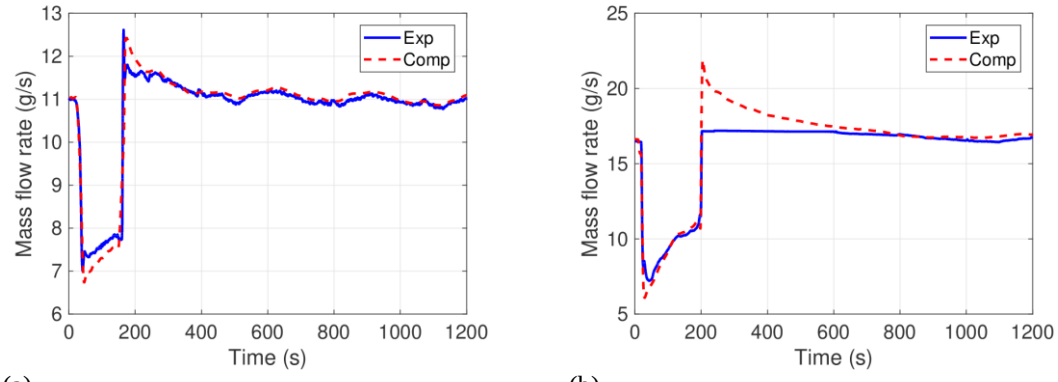

(a) (b)

Figure 9 – Comparison of the experimental and computed mass flow rate evolution in (a) HT0_07 and (b) HT0_10.

Another crucial model parameter in the heat slug propagation is the heat transfer coefficient between the hole and the bundle through the perforated portion of the central spiral. As described in [13], its value is larger than that obtained considering the ideal, unphysical condition of impermeable thin wall between the hole and the bundle, in the perforated portion of the spiral. As a result, also in this case a suitable multiplier > 1 is introduced in the 4C model, to account for the effects of local turbulence that can lead to a large deviation from the ideal, above-mentioned condition. This parameter, specific of each conductor and spiral geometry, has already been calibrated during the CSI test campaign [14] and analysis,

in particular for the proper simulation of the quench propagation [15]; therefore, being the conductor and spiral geometry of the CSM MU identical to those of the CSI, its value has been frozen (=10) for the current analysis. As reported in [15], the resulting steady state value of the heat transfer coefficient is (realistically) ~1000 W/m^{2}K across the spiral gap, to be compared to ~100 W/m^{2}K across the spiral wall. Moreover, also for other CICCs (as e.g. the EU DEMO conductor analyzed in [16]) show best-fitting value of that parameter between 10 and 20.

For all runs, 1300 s without any heat load are simulated before switching on the heater, in order to apply the heat load only when a self-consistent, steady state temperature profile within each hydraulic channel is reached.

IV.B.2. Results

As already done for the M_{IP} parameter, also in this case we examine the temperature difference with respect to the initial, steady state, unperturbed value, i.e. before the heater operation.

We considered the HT0_10 shot, because it features:

1. the nominal mass flow rate, i.e. ~16 g/s per DP;
2. a meaningful temperature increase, i.e. ~1 K (at least at the outlet of the directly heated DP);
3. a not-too-large flow chocking during the heater operation, as opposed to the heat slug with 300 W heater plateau, where the mass flow rate drops at ~ 0 g/s.

Note that for the first ~200 s the outlet temperature of all the selected sensors increases, both in the experiment and in the computed results, see Figure 10(a-b). This is due to the pressurization of the circuit as consequence of the sudden heat deposition.

The computed transit time, i.e. the time needed for the warm He slug to reach the outlet, is reproduced with good agreement with respect to the measured one.

The (average) error in this case is computed on the peak temperature reached at the outlet of the relevant DPs (for brevity, only the results on DP6-7 and DP8-9 are shown). The errors have been computed using Eq. (4) above. Figure 10(c) shows an agreement within 4% for all M_{IT} adopted. The resulting calibrated value for the IT multiplier is $M_{IT} = 0.10$. Note that the peak in the outlet temperatures is mildly dependent on $M_{IT,}$ but still an optimal value can be found. This could be due to the too fast response of the temperature, however this was the only type of transient thermal disturbance experiment.

This is clearly lower than the M_{IP} (= 0.29) computed above, even if the different thickness of the turn and pancake insulation are correctly taken into account. The calibrated parameters seem to show that the heat transfer through the turn insulation is worse than that through the IP insulation.

The explanation for this comes from the manufacturing process: the turn-to-turn gap is filled with the strips of Kapton-glass by insertion with no radial compression. During Vacuum Pressure Impregnation (VPI), the gap is filled with the epoxy. Concerning the pancake-to-pancake gap, it is filled with the glass cloth and the stacked pancakes are compressed during turn insulation. During VPI, the CSM is also compressed axially, but there is no radial compression. Therefore, the content of glass in the pancake-to-pancake gap is much higher than in the turn-to-turn gap, thus the heat transfer is higher between pancakes with respect to that between turns. Moreover, the nominal value of the temperature-dependent thermal conductivity adopted in the simulations is a fit of the measured thermal conductivity of a set of insulation materials with slightly different composition; therefore, the uncertainty on the nominal performance of the material is indeed partly depending also on its final, real composition.

The values of M_{IT} and M_{IP} are close to those found in other calibration exercises performed on other magnets. Typically, a single value for M_{IT} and M_{IP}, i.e., M_{ITIP}, was calibrated, finding $M_{ITIP} = 0.2$ for the KSTAR PF1 [10] and for the JT-60SA CS [11] and lower values in the range 0.12 – 0.17 for the ITER TFMC [9]. The present work is in agreement with the values found in other magnets and it additionally provides a distinction between the two contribution, i.e., IT and IP thermal coupling, showing that, depending on the manufacturing procedure, they can be quite different.

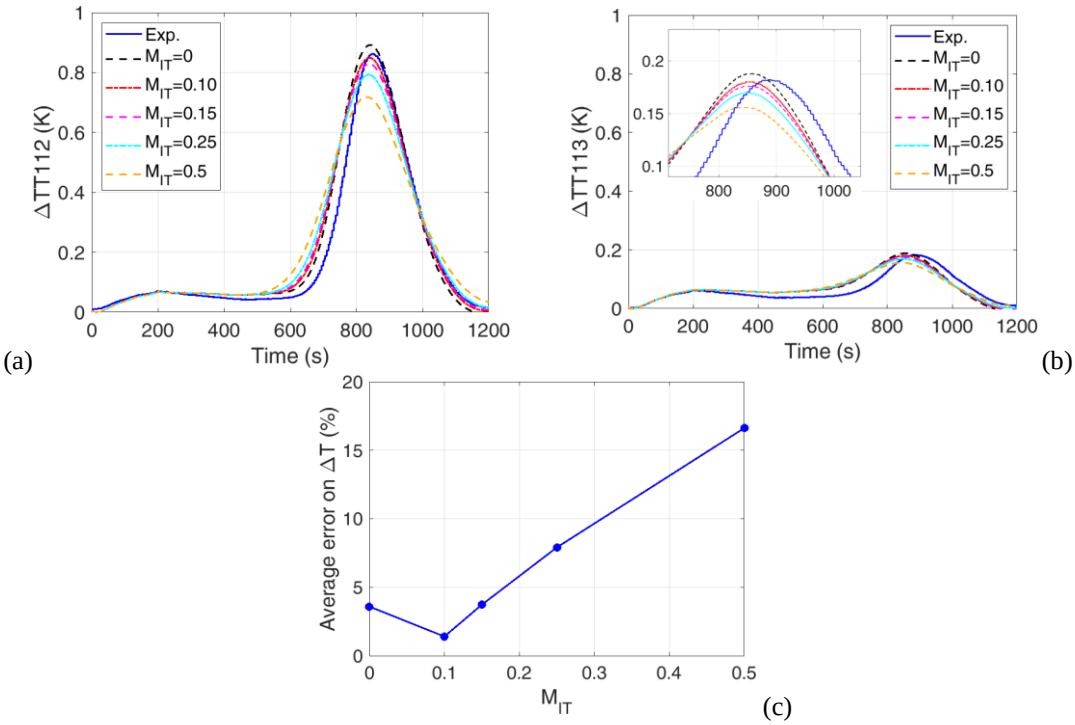

Figure 10 – Calibration of the IT thermal coupling multiplier M_{IT} on the shot HT0_10: comparison of the experimental temperature values (without the initial offset) for the sensors (a) TT112 (including a directly heated pancake) and (b) TT113 (including only indirectly heated pancakes), respectively, with those computed for different values of M_{IT}. The average error as a function of M_{IT} (c) is also shown.

IV.B.3. Validation

The M_{IT} calibration is validated against the measured outlet temperature of the shot HT1_07, which is a heat slug test performed firing the second heater.

The calibration of the IT thermal coupling is proven to be reliable, because the agreement between the measured and computed values is very good, i.e., the maximum error on the ΔT is < 0.1 K (less than 10% error on the temperature peak), see Figure 11.

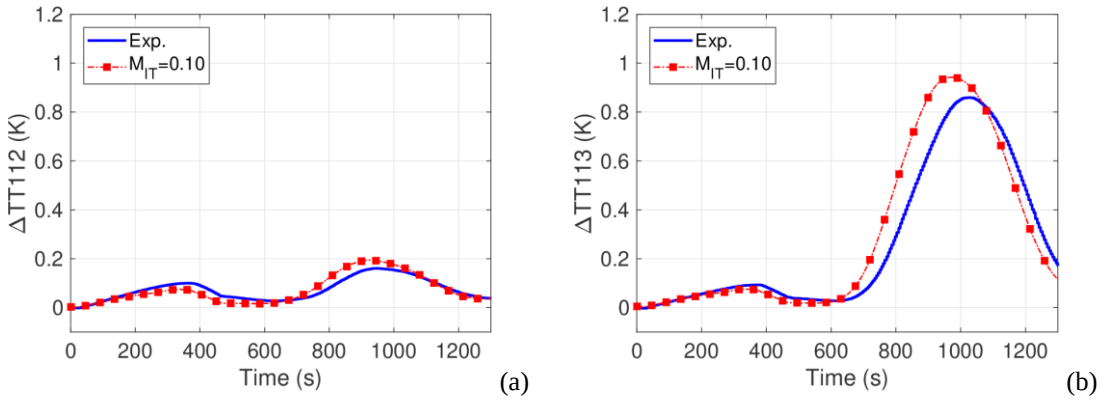

Figure 11 – Validation of the IT thermal coupling multiplier M_{IT} on the shot HT1_07. Comparison of the experimental trace (solid line) with the computed results (dash-dotted line + squares) for the sensors (a) TT112 (including a directly heated pancake) and (b) TT113 (including only indirectly heated pancakes), respectively, without the initial offset.

V. Validation of M_{IT} and M_{IP} on the CSM1 tests

The first CS module (CSM1) underwent an extensive test campaign at the beginning of 2020. Part of the tests were focused, as for the CSM MU, on the calibration of the TH tools to be employed in the analysis of the test results. However, it was also an opportunity to qualify the calibration previously obtained on the MU. Note that both the calibration and the qualification were possible against tests without current in the coil. The impact of the presence of current, thus of Lorentz forces on the inter-turn and inter-pancake thermal coupling was not assessed, since no thermal-hydraulic tests were carried out with charged coil.

Here we briefly show the level of agreement between computed and measured outlet temperature during a staircase heating scenario and during a heat slug test, aiming at the validation of the calibrated IP and IT multipliers, respectively. The agreement in both cases is good, i.e. within 0.1 K, see Figure 12 (10% error *at most* for both IP and IT).

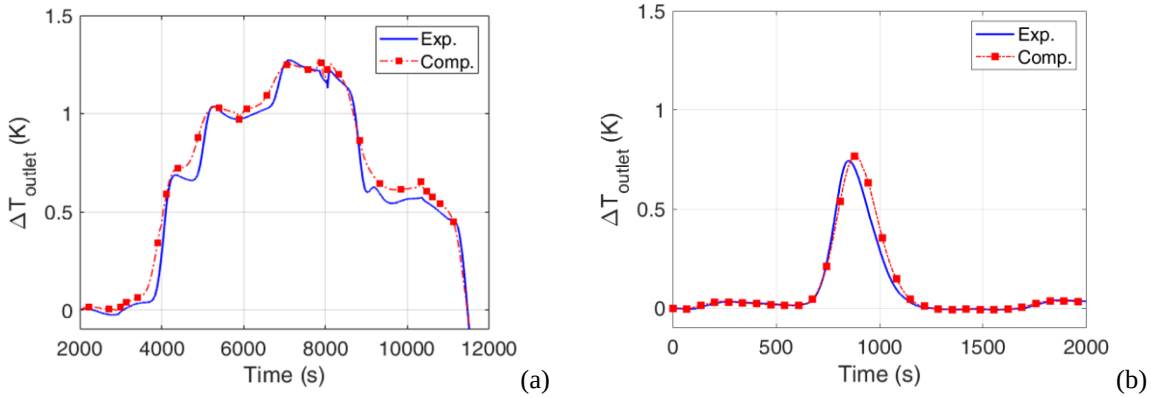

Figure 12 – Validation of the (a) IP and (b) IT thermal coupling multiplier on selected CSM1 TH tests comparing the measured and computed TT119 signal (outlet of the central DP). The selected tests are the long power steps performed on (a) February 20th, 2020 (10:30 AM) and (b) heat slug on January 28th, 2020 (3:40 PM).

VI. IP and IT heat transfer coefficient

A calibrated and reliable model can be used to extract relevant (macro) information on the heat transfer between turns and pancakes. Starting from the computed temperature profile along the heated conductor of the CSM1, see Figure 13, the power transferred among the turns in steady conditions can be extracted; the simulation of the long step of the heater power (adopted to calibrate the inter-pancake heat transfer) is used. The power can be computed as

$$q'(x) = M \cdot \frac{k_{ins}}{\delta_{ins}} P_w \cdot [T_1(x) - T_2(x)] \qquad (5)$$

where M is the calibrated multiplier, k_{ins} is the insulation thermal conductivity, δ_{ins} is the thickness of the insulation, P_w is the wetted perimeter, which corresponds to the side of the CICC, $T_1(x)$ and $T_2(x)$ are the temperature distribution of the (portion of) conductor considered.

An important information that can be extracted is the equivalent heat transfer coefficient (power per unit area transferred per unit of temperature difference): in the temperature range of interest in this analysis, i.e., 4.5-6.5 K, the heat transfer coefficient for turn-to-turn and pancake-to-pancake is in the range 2 - 8 W/m^2/K.

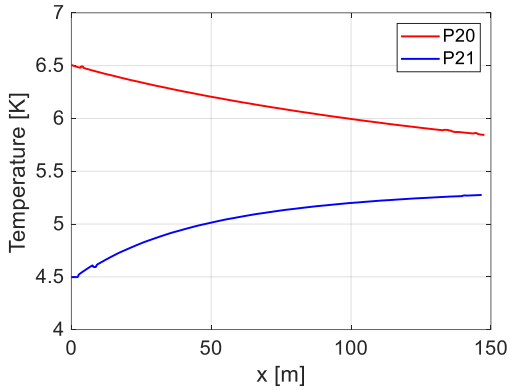

Figure 13 – Computed temperature profile at steady state along a heated (P20) and a non-heated (P21) hydraulic channel of CSM1, during the simulation of a long step of the heater power.

VII. Conclusions and perspective

Thermal-hydraulic numerical models are of paramount importance for the interpretation of the final tests designed for the qualification of the ITER magnets, as well as for the prediction of their behaviour during future operation. However, some specific free parameters of the thermal-hydraulic model of the CSM need dedicated calibration against experimental results: two of them, namely the multiplier for the inter-pancake heat transfer coefficient M_{IP} and the multiplier for the inter-turn heat transfer coefficient M_{IT} are considered here.

The calibration of the two free parameters to be used in the 4C thermal-hydraulic model of the CSM, developed and presented here, has been successfully performed thanks to the experimental data coming from the thermal-hydraulic test campaign performed on the mock-up in 2017. The calibrated values (M_{IP} = 0.29 and M_{IT} = 0.1), being significantly lower than 1, show that the simple recipe of considering the thermal resistance as given by the ratio of thickness over conductivity of the insulation around the jacket largely overestimates the heat transfer within the winding pack. This is expected, in view of the presence of contact thermal resistances between adjacent layers of insulation and motivates the need for the calibration.

The calibration of the 4C model of the mock-up has been also shown to be fully representative of the actual CSM winding pack.

In perspective, it would be good to assess the calibration of the heat transfer parameters also when the coil is electrically charged, i.e. when subjected to electro-magnetic forces, which could change the contact resistance and/or the thermal conductivity of the (multi-layer) insulation.

For the first time the 4C, one of the reference tools for the thermal-hydraulic analysis of superconducting magnet systems for tokamaks, has been rigorously calibrated and validated on an ITER magnet. The calibration has been successfully qualified, so that the model is now ready to be reliably applied to the simulation of operational transients.

Acknowledgement

The authors wish to thank the GA team for their kind hospitality during the MU and CSM1 tests and L. Savoldi for fruitful discussions regarding the analysis of the MU tests.

References

[1] N. Mitchell and A. Devred, "The ITER magnet system: configuration and construction status," Fus. Eng. Des. 123, 2017, pp.17-25

[2] J. P. Smith, J. Blanchard, A. Gattuso, R. Haefelfinger, R. Junge, K. Schaubel, S. Spitzer, W. Reiersen, "ITER Central Solenoid Module Fabrication," 2013 IEEE 25th Symposium on Fusion Engineering (SOFE), San Francisco, CA, 2013, pp. 1-4.

[3] L. Savoldi Richard, F. Casella, B. Fiori and R. Zanino, "The 4C Code for the Cryogenic Circuit Conductor and Coil modeling in ITER", Cryogenics, vol. 50, pp. 167-176, 2010.

[4] L. Savoldi and R. Zanino, "M&M: Multi-Conductor Mithrandir Code for the Simulation of Thermal-Hydraulic Transients in Superconducting Magnets", Cryogenics, vol. 40, pp. 179-189, 2000.

[5] R. Bonifetto, F. Casella, L. Savoldi Richard and R. Zanino, "Dynamic modeling of a SHe closed loop with the 4C code," AIP Conference Proceedings: Advances in Cryogenic Engineering, vol. 1434, 2012, pp. 1743-1750.

[6] E. Mattsson, H. Elmqvist and M. Otter, "Physical system modeling with Modelica", Control Engineering Practice, vol. 6, pp. 501-510, 1998.

[7] http://www.tlk-thermo.com/ date accessed, March 20, 2018.

[8] R. Bonifetto, A. Brighenti, T. Isono, N. Martovetsky, K. Kawano, L. Savoldi, R. Zanino, "Analysis of the cooldown of the ITER Central Solenoid Model Coil and Insert Coil", Superconductor Science and Technology, vol 30, p. 015015, 2017.

[9] R. Zanino, R. Bonifetto, R. Heller, and L. Savoldi Richard, "Validation of the 4C thermal-hydraulic code against 25 kA safety discharge in the ITER toroidal field model coil (TFMC)," IEEE Trans. Appl. Supercond., vol. 21, no. 3, pp. 1948–1952, Jun. 2011.

[10] L. Savoldi Richard, R. Bonifetto, Y. Chu, A. Kholia, S.H. Park, H.J. Lee and R. Zanino, "4C code analysis of thermal-hydraulic transients in the KSTAR PF1 superconducting coil," Cryogenics, vol. 53, 2013, pp. 37-44.

[11] R. Bonifetto, L. Savoldi and R. Zanino, "Thermal-Hydraulic Analysis of the JT-60SA Central Solenoid Operation," IEEE Transactions on Applied Superconductivity, vol. 29, 2019, Art. ID 4201005.

[12] F. Gauthier, T. Schild, N. Martovetsky, K. Khumthong, K. M. Schaubel, J. Sheeron, A.R. Langhorn, R. Bonifetto, R. Zanino, A Zappatore, "Thermal hydraulic behavior of the first ITER CS Module", IEEE Transactions on Applied Superconductivity, vol. 31(5), 2021, 4201105.

[13] R. Zanino, S. Giors and L. Savoldi Richard, "CFD model of ITER CICC. Part VI: Heat and mass transfer between cable region and central channel", Cryogenics, vol. 50, pp. 158-166, 2010.

[14] N. Martovetsky, T. Isono, D. Bessette, A. Devred, Y. Nabara, R. Zanino, L. Savoldi, R. Bonifetto, P. Bruzzone, M. Breschi, L. Zani, "Characterization of the ITER CS conductor and projection to the ITER CS performance", Fusion Engineering and Design, vol 124, pp 1-5, 2017.

[15] R. Bonifetto, T. Isono, N. Martovetsky, L. Savoldi and R. Zanino, "Analysis of Quench Propagation in the ITER Central Solenoid Insert (CSI) Coil", IEEE Transactions on Applied Superconductivity, vol. 27, Art. ID 4700308, 2017.

[16] R. Bonifetto, P. Bruzzone, V. Corato, L. Muzzi, L. Savoldi, B. Stepanov, R. Zanino, and A. Zappatore, "Thermal–hydraulic test and analysis of the ENEA TF conductor sample for the EU DEMO fusion reactor," IEEE Transactions on Applied Superconductivity, vol. 28(4), 2018, 4205909.